Surface parametric influences on the photocatalytic behaviour of zinc oxide nanoparticles

R. Jagadeeswari[a], G. Rathika[b], K. V. Satheesh Kumar [c], P. Selvakumar [d,*]
[a]*Department of Chemistry, KPR Institute of Engineering and Technology, Coimbatore-641407, India*
[b]*Department of Chemistry, PSG College of Arts & Science, Coimbatore -641014, Tamilnadu, India*
[c]*Department of Mechanical Engineering, Kongu Engineering College, Perundurai 638052, Tamilnadu, India*
[d]*Department of Humanities and Sciences, Gokaraju Rangaraju Institute of Engineering and Technology, Hyderabad, 500090, Telangana, India*

Zinc oxide nanoparticles were chemically synthesised and characterised by UV-DRS spectroscopy, FTIR, scanning electron microscopy with energy-dispersive X-ray diffraction, and X-ray powder diffraction. In order to evaluate the impact of the synthesis process on the structural parameters, Rietveld refinement was done using the GSAS-II programme on experimentally acquired XRD data. ZnO was found to have a hexagonal structure with lattice parameters of a = b =3.247 Å; c = 5.205Å and an average size of about 20-40 nm, as determined by Rietveld refinement of XRD and SEM data. FTIR and EDX analysis was used to confirm the functional group and elemental composition of ZnO NPs. The UV-DRS spectra revealed that the synthesised ZnO had an optical band gap of 3.05 eV. Parametric investigations of the surface morphology of ZnO nanostructures were conducted using the Gwyddion programme. Pseudo-first-order rate kinetics were observed for the photodegradation of two cationic dyes, MB (87.87%) and RhB (74.79%), in the presence of UV light.

(Received November 3, 2023; Accepted February 12, 2024)

Keywords: ZnO, Surface parameters, Morphology and DFT studies

1. Introduction

Due to their advantageous electrical and optical characteristics in the fabrication of nano scaled optoelectronic and electronic devices with many functionalities, nano sized semiconductors have become increasingly important in today's world. Zinc oxide, often known as ZnO, stands out among other semiconductors, since at room temperature it has a large straight band gap of 3.37 eV and a significant exciton binding energy of 60 meV [1]. The chemical, electrical, optical, and biological properties of nanoparticles may be influenced by tailoring their size and shape. Changing the precursors and reducing agents used in synthesis is a simple technique to manipulate nanoparticle size and form. Changing the ratio of precursors to reducing agents is a straightforward technique to alter the size and form of synthesised nanoparticles. The fast synthesis of nuclei made possible by strong reducing agents like sodium hydroxide and sodium borohydride ($NaBH_4$) results in nanoparticles with a narrow size distribution and a small average crystallite size. Trisodium citrate (TSC) and other weak reducing agents, on the other hand, produce nanoparticles of quite large and a wider size dispersion [2]. So as to control the dimensions of metal oxide nanoparticles, researchers have looked at a variety of reducing agents using biological and chemical methods [3]. The employment of chemical reducing agents and stabilising agents to avoid agglomeration is essential to the chemical synthesis process. To prevent clumping, chemical reducing agents and stabilising agents are used due to the chemical nature of the synthesis. Particle

* Corresponding author: selvakumarpresec@gmail.com
https://doi.org/10.15251/JOR.2024.201.115

size and shape are two of the most important physical parameters that influence nanoparticles chemical, electrical, optical, and biological capabilities. The pore structure facilitates ion diffusion from the electrolyte, which improves the kinetic interaction and the capacity for charge storage.

In this study, the structure and surface morphological features of ZnO NPs produced by chemical synthesis were reported. ZnO NPs surface characteristics were investigated for their potential in the degradation of cationic dyes like MB and RhB.

2. Experimental

2.1. Materials

Merck Specialties Private Limited, Mumbai supplied the AR grade Zinc acetate dihydrate, sodium hydroxide, rhodamine b, and methylene blue were used as such without further purification. All aqueous extracts and solutions used in the experiments were prepared using double-distilled water.

2.2. Preparation of ZnO nanoparticles

The preparation of ZnO-NPs was done using earlier reported studies [4]. Zinc acetate dihydrate (0.2M) was mixed with 70 mL of distilled water and agitated for several minutes until completely dissolved. Following the addition of 30 ml of sodium hydroxide, then the mixture was homogenised and heated to 60°C for two hours. It was then cooled to ambient temperature and centrifuged for ten minutes. The precipitate that was produced was rinsed with ethanol once and then again with distilled water before being collected. The obtained precipitate had an off-white colour after being water-evaporated at 100°C and then calcinated in a furnace at 500°C for 2 hours.

2.4. Characterisation and measurements

X-ray diffraction (XRD) experiments were performed using an X-ray diffractometer (Bruker Advance) and CuKα radiation (1.5406Å) was used to determine the crystal structure of ZnO nanoparticles. The morphology and elemental content of ZnO NPs were examined using a scanning electron microscope (SEM with EDX, Zeiss). In addition, the surface roughness was analysed using the free programme Gwyddion. Using Gwyddion 2.58, the SEM pictures of ZnO nanoparticles were transformed into three-dimensional images. Then, the following roughness characteristics were determined: mean roughness (Ra), mean square roughness (Rq), surface skewness (Rsk), and kurtosis coefficient (Rku)[5]. A UV-VIS spectrophotometer was used to record the optical absorption spectrum of the nanoparticles (JASCO V-570).

2.5. Photocatalytic studies

As a photocatalytic reactor system, the wooden chamber was utilised for testing photodegradation. Philips TUV-08 UV light (15W, λ-365 nm) was placed inside the wooden enclosure. 0.03 g of ZnO catalyst was dissolved in 30 mL of 100 μm dye aqueous solution (RhB & MB). After being stirred for 10 minutes, the solution was left undisturbed for an additional hour in the dark to allow for adsorption equilibrium to be reached. Once the sample solution was ready, it was sent to the photoreactor to be exposed to UV light. Around 5 mL of a catalyst and dye solution mixture were added, and the UV light was turned on. For 60 minutes at room temperature, the ZnO NPs dye solution was subjected to UV light.

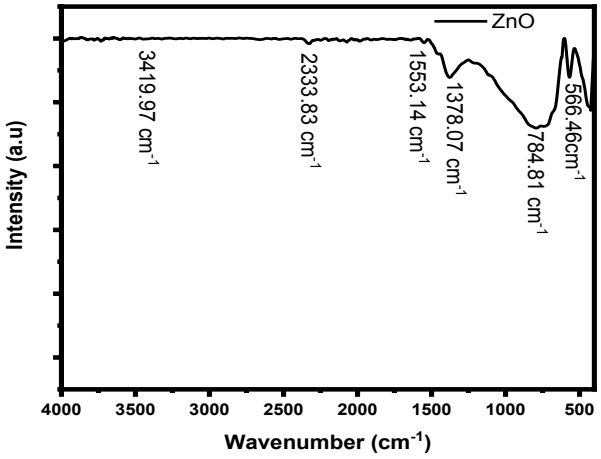

Fig. 1. FTIR spectra precipitated ZnO NPs.

3. Result and discussion

3.1. Vibrational spectroscopy

FTIR was recorded at room temperature to determine the predominant functional group of the catalyst. The FTIR spectra of ZnO nanoparticles are shown in Figure.1 and peaks at 566.46 and 784.81 cm^{-1} are due to Zn-O bond stretching vibrations. The crystalline nature of the ZnO photocatalyst is reflected in the broadness of a peak, and the absorption band at 2333.83 cm^{-1} is created by the asymmetric and symmetric stretching mode vibrations of an air-absorbed CO_2 molecule[9]. Also, the wide peak at 3419.97 cm^{-1} and 1378.07 cm^{-1}, 1553.14 cm^{-1} may be due to stretching and bending vibrations of– OH group absorbed from the environment on the surface of the catalyst during FTIR measurement[10].

3.2. Optical and bandgap calculation

UV–DRS of ZnO NPs was measured in the wavelength range of 200 to 500 nm, as shown in Figure.2a. A wide absorption peak is found between 200 and 400 nm in DRS absorption spectra, The maximum absorbance was observed at 332 nm and the optical band gap of the produced ZnO NPs was determined using Tauc's equation[11].

$$[F(R)h\upsilon/t]^{1/n} = A\,(h\upsilon - E_g) \tag{2}$$

where F(R)-Kubelka–Munk function[12] ($F(R) = (1-R)^2/2R$), 't'-thickness of the material, R-Reflectance of the spectrum, n-band gap transition, A-proportional constant, and $h\upsilon$-photon energy. Figure.2b. depicts Tauc's plot between the relationship of energy and $[F(R)h\upsilon]^2$ and the tangent line drawn to meet the x-axis line. Based on the Figure.2b., the energy band gap (Eg) for ZnO NPs was calculated to be 3.05 eV. Therefore, the energy gap widens when particle size decreases owing to Quantum size effects on electrical energy bands of semiconductors. When the nano crystallite size is less than the Bohr radius of the bulk excitation, it becomes more noticeable. Holes and electrons interacting in a columbic fashion are particularly important in nano sized materials. Valence and conduction bands in semiconductors may be altered via quantum confinement of the following equation may be used to compute the valence band (VB) edge potential of a semiconductor at zero charge.

$$E_{VB} = X - E^C + 0.5\,E_g \tag{3}$$

where E_{VB} is the VB edge potential, X is the semiconductor's electronegativity, E^c is the energy of free electrons on the hydrogen scale (about 4.5 eV), and E_g is the semiconductor's band gap energy. The conduction band (CB) edge potential (E_{CB}) may be calculated using the formula E_{CB} =

E_{VB} -E_g. The X value for ZnO is about 5.79, and its E_{VB} and E_{CB} have been determined to be 2.815 eV and -0.235 eV, respectively. Changes in the band gap energy and blue shift in the UV-vis spectrum strongly indicate that the particle size of the catalyst has reduced.

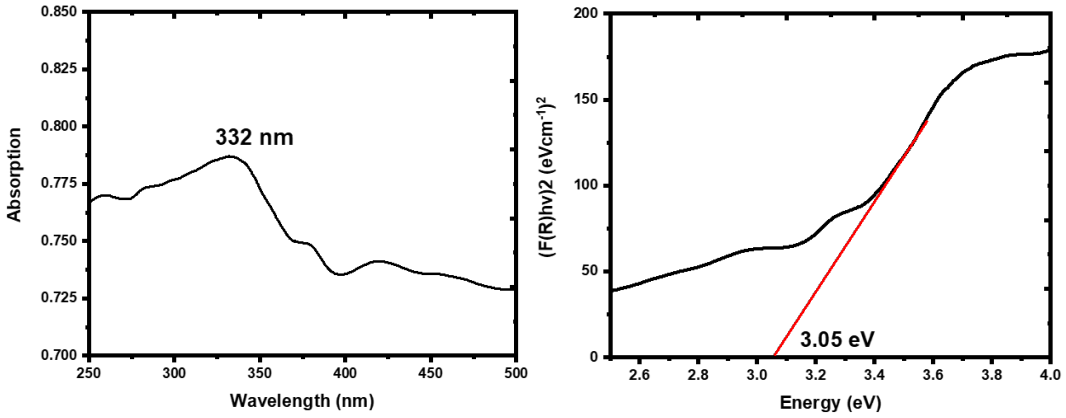

Fig. 2. (a) Absorbance Spectra; (b) Tauc's Plot for precipitated ZnO NPs.

3.3. Size and structure

PXRD is a crucial method for determining the structure, elements phase and type of elements present in ZnO NPs. In addition, the ZnO NPs crystallite size may be determined using PXRD data. Diffraction patterns of ZnO NPs, was observed with 2θ ranging from 20^o to 80^o, was shown in Figure.3. Based on the PXRD pattern, the peaks have emerged at the angle 2θ of (37.26^0, 43.31^0, 62.9^0, 75.42^0, and 79.38^0), which corresponds to the planes (111), (200), (220), (311) and (222) and is agreed well with JCPDS card no.36-1451[13].

This result indicates that the produced nanoparticles contain a ZnO phase and a hexagonal crystal structure. The strength and sharpness of the peaks demonstrate the crystalline character of the produced ZnO NPs. In addition to this, no further peaks were found, indicating the purity of the ZnO NPs. Using standard Scherrer formula[14] (eqn.4), the average crystallite size of as-prepared ZnO NPs was determined to be 25.2 nm.

$$D = \frac{K\lambda}{\beta cos\theta} \tag{4}$$

where D-average crystallite size, λ-wavelength of the incoming radiation (in this case, Cu Kα with a wavelength of 1.540 Å), K-constant (0.89), often known as the shape factor, β-FWHM, and θ-diffraction angle. Using the formula provided below(eqn.5)[15],

$$\delta = \frac{1}{D^2} \tag{5}$$

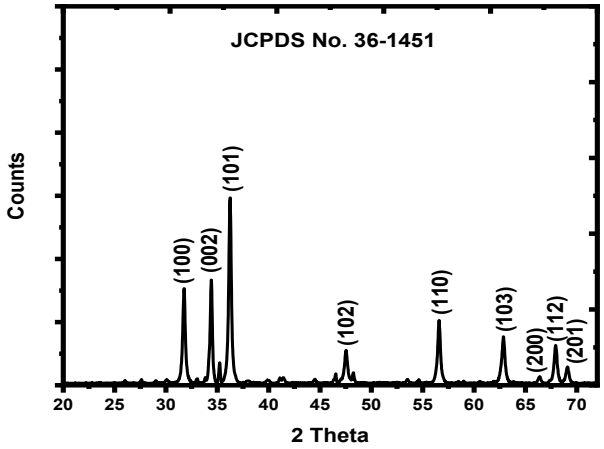

Fig. 3. XRD patterns of precipitated ZnO NPs.

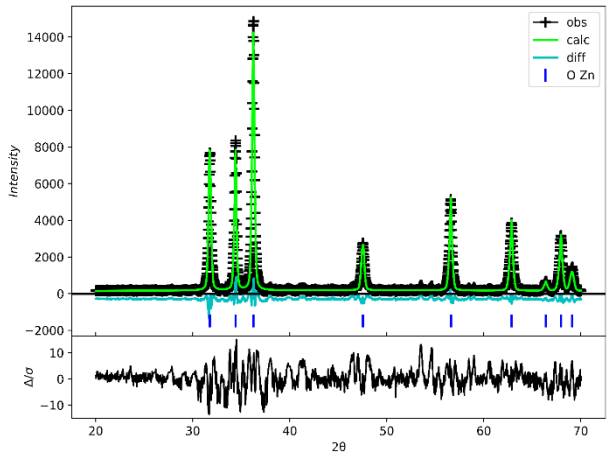

Fig. 4. Rietveld refinement of precipitated ZnO NPs.

The dislocation density (δ) was computed and found to be 1.56×10^{15}. The PXRD strain can also be evaluated from Williamson-Hall (W-H) formula ($\varepsilon = \beta\cos(\theta)/4$)[16]. Stress can be obtained from the strain according to Hooke's law ($\sigma = C\varepsilon$). Where, 'C'-bulk young's modulus (1.46 ± 10^{10} N/m^2). The value of strain and stress is found to be 0.00136 and 19.91 MPa for ZnO NPs. Furthermore, the X-ray density was evaluated using formula(eqn.6) and found to be 5.77g/cm^3

$$\rho = \frac{nA_w}{V_{cell}N_A} \tag{6}$$

where, n is effective number of atoms per unit cell, A_w is atomic weight, $V_{cell}$is volume of unit cell (for HCP 6 x$\sqrt{3}$/4 x a^2 x c), N_A is Avogadro's number. Various aspects of the XRD pattern, such as peak asymmetry, broadening, shift, etc., may be employed with the Rietveld refinement technique[17] to analyse structure of the investigated crystal material. In the current work, Rietveld refinement is performed on experimentally collected XRD data through GSAS-II program in order to evaluate the effect of synthesis process on physical parameters (Figure.4.). It was performed by pseudo- Voight function which uses the integrated diffraction peaks as a function of structural characteristics and the Marquardt least squares approach was applied to refine the data, it reduces the disparity between calculated and experimental pattern. Refinement provides exact fittings for the peaks observed with standard patterns of pure ZnO (JCPDS card no.36-1451) with negligible refinement errors[18]. The improved parameters and estimated significant factors are given in Table 1.

Table 1. Rietveld refinement parameters of ZnO NPs.

Structural parameters	Rietveld refined		
Crystal Structure	Hexagonal		
Lattice constant (Å) a=b	3.247		
C	5.205		
Unit-cell volume (Å3)	47.55		
Space group	P63mc		
Density (g/cm3)	5.684		
χ^2	13.77		
Rwp (%)	15.92		
RF(%)	4.118		
Rp (%)	9.55		
Atomic Position	x	y	z
Zn1	0.333	0.666	0
O1	0.333	0.666	0.375

3.4. SEM-EDS

As can be seen in the SEM pictures of ZnO NPs shown in Figure.5a, the particles of ZnO tend to agglomerate, resulting in an irregular spherical form with particles of varied sizes possessing a larger surface area and it performed well in photocatalytic assays[19].

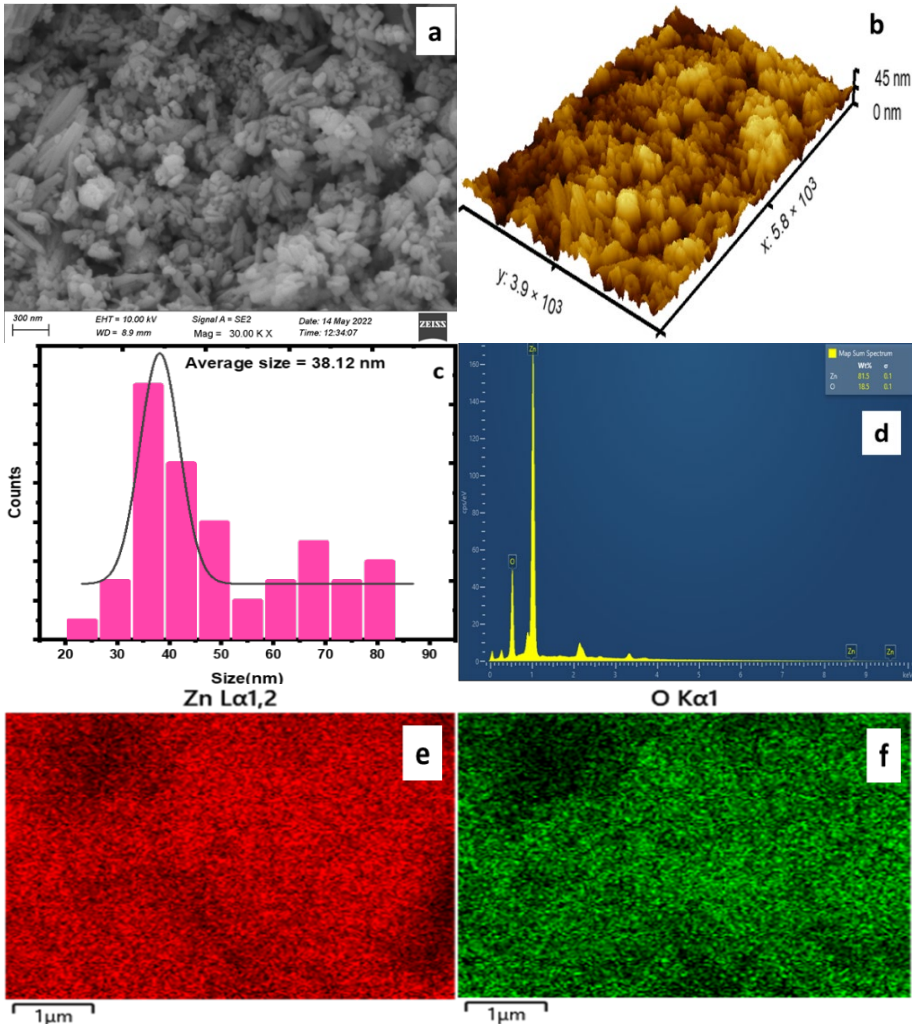

Fig. 5. (a and b) SEM image and SEM derived nanocrystal size; (c) 3D SEM image; (d) EDX spectra; (e and f) element mapping of ZnO NPs.

The 3D representation of SEM picture of ZnO NPs, shown in Figure.5b, has nanoscale growth sites distributed across the surface (see Figure.5c). In addition, numerous crystallites with a pointed cone form were found. ZnO NPs EDX is seen in Figure.5d. Clearly, Zn and O make up the synthesised NPs. ZnO nanoparticle elemental mapping, seen in Figures 5e and 5f. Since no other contaminants were found in the spectrum of ZnO NPs, this provides more evidence that ZnO NPs are clean[20]. The precise atomic proportions of the elements Zn and O are 81.5% and 18.5%, respectively.

3.5. Surface parametric studies

Gwyddion is the SEM analysis application that is both the most user-friendly and compatible with several platforms. Gwyddion offers four parameters for assessing surface features, including the mean roughness (Ra), which reflects the average value of the surface roughness of the sample, the mean square roughness (Rq), which defines the considerable change in the surface roughness of the ZnO NPs, the surface skewness (Rsk), which is used to represent the distribution symmetry of the surface height of ZnO NPs, and the kurtosis coefficient (Rku), which describes the deciding to display a 3D view of the data results in a 3D image of the data depicting the surface structure on the plane, as shown in Figure.5b, together with the loaded 2D photographs indicating the height of the surfaces(Figure.5c). Ra values for ZnO NPs averaged 49 nm, indicating that the produced particles had a rather rough surface since the calcination process had increased their height[15].

As an indicator of surface roughness, the average Rq value for ZnO NPs is 102.4 nm. A negative result for surface skewness (Rsk) of -0.489 implies that there is a greater proportion of low points (troughs) than high points (peaks) (i.e., there is more area where the sample surface height is above the mean value). ZnO NPs had a Rku value of 2.39, which was used to graphically represent the wavy characteristics of the surface height distribution. Rougher surfaces are often better for interacting with liquids and solids because they have a larger contact area.

ZnO NPs activity is proportional to their size and shape. Bandgap energy of 3.05 eV based on UV-DRS data. Surface area is also greatly affected by shape. In addition, the SEM findings on the surface roughness provide validity to ZnO's superior activity. Since adsorption is the first stage in the photocatalytic process, the dye moiety will be able to sit readily on the surface of the catalyst if the roughness is high owing to poor crystallinity, resulting in Ra about 84.8 nm and Rq around 102.4 nm. Therefore, the results of this investigation demonstrate unequivocally that the generated ZnO NPs ability for photocatalytic activity and other catalytic-like activities depend critically on their particle size, surface area, and shape.

3.6. Photocatalytic degradation of MB and RhB

Under UV light, the photocatalytic performance of ZnO was investigated using RhB and MB dyes. Figure.6a. & 6b. depict the degradation of MB dye by ZnO NPs at various time intervals. The prominent absorption peak of MB & RhB (663 nm & 554 nm) in absorption spectra declines gradually. In the presence of ZnO NPs, practically more than 85% of MB dye was destroyed under UV light within 60 min. Figure.6a. & 6b. illustrates the effectiveness with which ZnO NPs degrade dyes. ZnO NPs reached efficiency of degradation as 87.87% (MB dye) and 74.79% (RhB) in 60 min. The greater photocatalytic activity of ZnO NPs suggests a rise in degradation efficiency, which might be attributable to the increase in total surface area. This refers to the quantity of the photocatalyst surface reactive sites(surface roughness) for the production of free radical[16]. The added cause for the rise in photocatalytic activity was the semiconductor's narrower band gap(3.05 eV), which allows it to produce further photons to stimulate electrons from the valence band to the conduction band[17]. The arrangement of the electronic band structure of the ZnO NPs also affects the photocatalytic activity. In order to strengthen these findings, plausible degradation mechanism and kinetic study were included. The surface roughness of ZnO NPs has played a crucial role in the photodegradation of dyes.

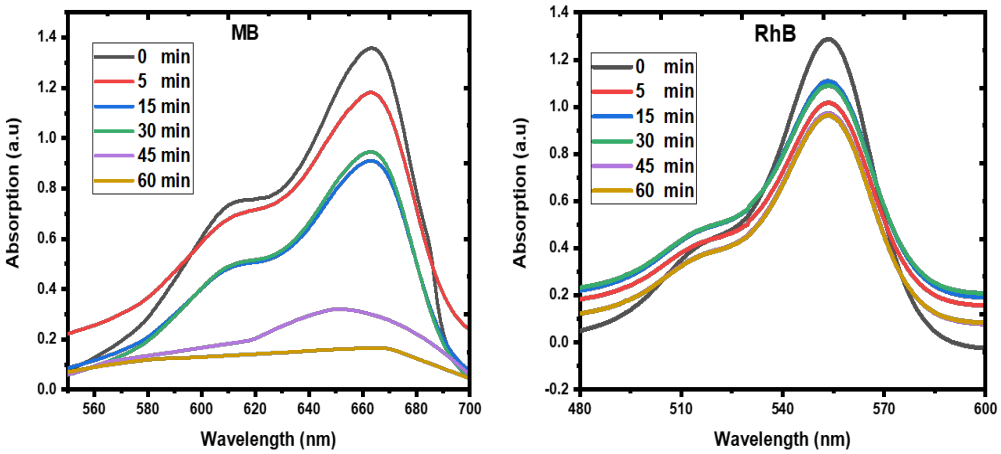

Fig. 6. (a and b) Photocatalytic activity of precipitated ZnO NPs against MB and RhB under UV light.

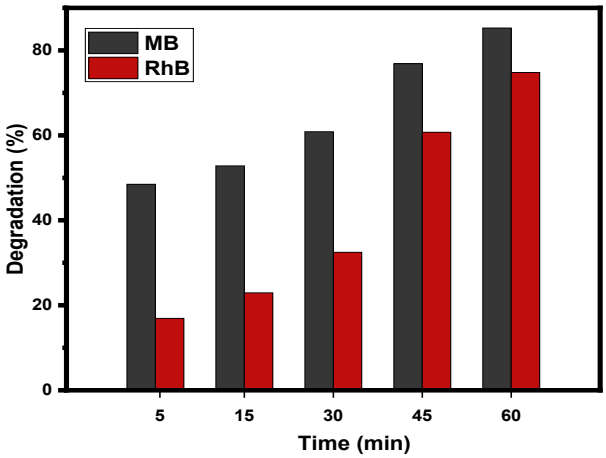

Fig. 7. Degradation efficiency of MB & RhB under UV light by ZnO NPs.

3.7. Degradation mechanism and kinetic study

Ultraviolet light causes electrons in ZnO's valence band (the lowest energy level) to gather momentum and jump to the excited state, where higher energies prevail (conduction band). The amount of energy required is equal to the bandgap energy of the nanomaterial. According to the UV-DRS analysis, ZnO has an energy bandgap value of 3.05 eV. So, when excited, the holes in the valance band may freely mix with water molecules to produce OH free radicals, which can then repeatedly attack the target chemical moiety (RhB & MB), eventually destroying it.

The comparative degradation efficiency of MB and RhB dyes is shown in Figure.7, and Figure.8a & 8b. depicts the relationship between concentration changes and reaction time. The inset Figure.8a & 8b., a schematic illustration of the photocatalytic generation of free radicals by ZnO. The rate constant is determined using the following formula(eqn.7) and the degradation process follows pseudo-first-order kinetics.

$$-ln\left[\frac{C}{C_0}\right] = kt \tag{7}$$

To determine the R^2 value and the rate constant (k), a graph between ln (C/Co) and response time. Further the R^2 value and rate constant (k) are calculated to be 0.9800; 0.9440 and 0.0325 min^{-1}; 0.0216 min^{-1} for MB and RhB.

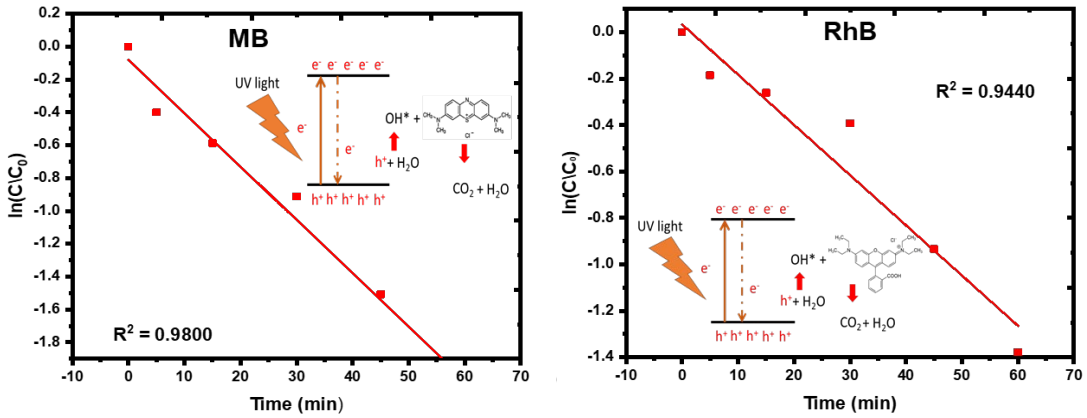

Fig. 8. (a and b) Pseudo first order kinetics for photocatalytic degradation of MB & RhB of precipitated ZnO NPs.

4. Conclusion

Nano ZnO was effectively synthesised by soft chemical method, and their structure and shape were analysed using a physicochemical method. The particle size range that was found by the PXRD experiments (20-40 nm) is validated by the scanning electron microscopy (SEM). Pure ZnO NPs were synthesised, as confirmed by EDX analysis, which showed a sharp peak and no traces of any other elements. The computed optical band gap of 3.0 eV is consistent with the nature of ZnO nanoscale production, and X-ray diffraction examination validated the hexagonal crystal structure and the point group P63mc was confirmed by the Rietveld refinement technique. The particle size and narrow band gap of ZnO NPs, as observed in SEM pictures using Gwyddion, may account for the efficient removal of RhB and MB dyes from their aqueous solutions by photodegradation. Photocatalytic degradation of MB dye reached 87.87% and RhB 74.79% in 60 minutes. The rate of photodegradation of MB and RhB is characterised by pseudo-first-order reaction kinetics.

References

[1] M. Akbarian, S. Mahjoub, S. M. Elahi, E. Zabihi, H. Tashakkorian, New J. Chem., vol. 42, no. 8, pp. 5822-5833, 2018; https://doi.org/10.1039/C8NJ00496J

[2] V. Trovato et al., Polymers, vol. 14, no. 14, p. 2788, 2022; https://doi.org/10.3390/polym14142788

[3] A. Saka et al., J. Nanomater., vol. 2022, 2022; https://doi.org/10.1155/2022/6230298

[4] S. A. Al-Ghamdi et al., Res. Chem. Intermed., vol. 48, no. 11, pp. 4769-4783, 2022; https://doi.org/10.1007/s11164-022-04845-z

[5] Y. Ghiyasi, E. Salahi, H. Esfahani, Mater. Today Commun., vol. 26, p. 102163, 2021; https://doi.org/10.1016/j.mtcomm.2021.102163

[6] M. Akbarian, S. Mahjoub, S. M. Elahi, E. Zabihi, H. Tashakkorian, Colloids Surf. B Biointerfaces, vol. 186, p. 110686, 2020; https://doi.org/10.1016/j.colsurfb.2019.110686

[7] A. S. Abdelsattar, W. M. Farouk, S. M. Gouda, A. Safwat, T. A. Hakim, A. El-Shibiny, Mater. Lett., vol. 309, p. 131344, 2022; https://doi.org/10.1016/j.matlet.2021.131344

[8] A. M. Abioye, Z. A. Noorden, F. N. Ani, Electrochimica Acta, vol. 225, pp. 493-502, 2017; https://doi.org/10.1016/j.electacta.2016.12.101

[9] M. Akbarian, S. Mahjoub, S. M. Elahi, E. Zabihi, H. Tashakkorian, Mater. Res. Express, vol. 6, no. 9, p. 095022, 2019; https://doi.org/10.1088/2053-1591/ab2c49

[10] A. Saranya, A. Murad, A. Thamer, A. Priyadharsan, P. Maheshwaran, ChemistrySelect, vol.

6, no. 16, pp. 3995-4004, 2021; https://doi.org/10.1002/slct.202100413

[11] S. K. Ahmed, M. F. Mahmood, M. Arifuzzaman, M. B. Hossen, Results Phys., vol. 30, p. 104833, 2021; https://doi.org/10.1016/j.rinp.2021.104833

[12] B. Thrope, A. R. Ferreira Lima, A. H. Pinto, J. Chem. Educ., vol. 99, no. 5, pp. 2055-2066, 2022; https://doi.org/10.1021/acs.jchemed.1c00831

[13] T. T. Truong, T. T. Khieu, T. H. T. Nguyen, T. T. Nguyen, VNU J. Sci. Nat. Sci. Technol., vol. 38, no. 3, 2022.

[14] A. G. Ramu, M. A. Kumari, M. S. Elshikh, H. H. Alkhamis, A. F. Alrefaei, D. Choi, Chemosphere, vol. 271, p. 129475, 2021; https://doi.org/10.1016/j.chemosphere.2020.129475

[15] V. Bueno, A. Bosi, T. Tosco, S. Ghoshal, J. Colloid Interface Sci., vol. 606, pp. 480-490, 2022; https://doi.org/10.1016/j.jcis.2021.07.142

[16] H. Sadiq et al., J. Mol. Liq., vol. 335, p. 116567, 2021; https://doi.org/10.1016/j.molliq.2021.116567

[17] M. Shabaani, S. Rahaiee, M. Zare, S. M. Jafari, Lwt, vol. 134, p. 110133, 2020; https://doi.org/10.1016/j.lwt.2020.110133